Spatial distribution of vortices and metastable states in rotating He II

P. Mathieu, J. C. Marechal, and Y. Simon
Groupe de Physique des Solides de l'Ecole Normale Supérieure, 75231 Paris Cedex 05, France
(Received 25 February 1980)

Accurate measurements of the attenuation of second sound in rotating rectangular cavities are reported. By driving different resonant modes of the cavity, we obtained information about the spatial distribution of vortices. The theory of stable and metastable states in deformed rotating cylinders is developed in the limit of many vortices, then tested by experiment in the high-velocity range. Metastability and hysteresis phenomena are observed in the whole investigated range of angular velocities ($\Omega \sim 10^{-2}$ to 10 $\sec^{-1}$). At a given Ω, the observed vortex number N can fluctuate around the equilibrium value N_0: $\Delta N/N_0 \lesssim 10\%$ for $\Omega \gtrsim 1$ $\sec^{-1}$; $\Delta N/N_0 \sim 1$ for $\Omega \lesssim 10^{-1}$ $\sec^{-1}$. Primarily, thanks to a good temperature stabilization, we were able to distinguish and systematically reproduce three vortex states for any value of Ω: the thermodynamic equilibrium N_0 state, and two limiting metastable states containing, respectively, the minimum number N_1 and the maximum number N_2 of vortices. In the high-velocity range, ΔN can be related to a variation of the thickness d of the vortex-free strip occurring near the walls; d varies between two extremal values d_1 and d_2, which turn out to be independent of the boundary geometry. The role of mechanical vibrations is discussed, and the hyrdodynamic predictions concerning the barrier energy are reconsidered in relation to these experiments. From the low-velocity results, it emerges that the experimental value of the critical angular velocity is in substantial disagreement with theory.

I. INTRODUCTION

The motion of He II in a rotating vessel according to the two-fluid model is well known.[1] The normal fluid is carried along with the walls of the container like a classical fluid, whereas the superfluid only mimics solid-body rotation thanks to a system of quantized vortex lines parallel to the axis of rotation. Simply to detect vortices, then to investigate their spatial distribution, two phenomena associated with vortices have been extensively exploited: electron trapping,[2–5] and attenuation of second sound.[6,7]

The electron-trapping method consists in decorating the vortex axes with electrons produced by a radioactive source. This ingenious experiment permits single vortex lines to be detected, and, by extracting the trapped electrons through the liquid meniscus, the spatial positions of vortices can be directly visualized. Unfortunately, numerous difficulties arose in improving this technique. As pointed out by the authors,[3,4] a number of vortex lines may not be recorded, perhaps because they do not terminate at the free surface. Furthermore, in order to produce photographs[4] of films,[5] it is necessary to work at temperatures lower than 0.3 K, where it seems difficult to get a stable array of vortices. However, very recently, stable and complete patterns of a small number of vortices ($N \sim 1$–10) have been recorded.[5]

The second-sound method, which is the one we used in the present work, utilizes the fact that vortices give rise to an extra attenuation of the second sound. A closed cavity serves both as rotating vessel and second-sound resonator. Each vortex in the cavity contributes to the damping of the second-sound wave proportional to the squared wave field. Therefore, a vortex will act differently if it is located near a node or near an antinode of the standing wave. So, by studying various modes of the cavity, we clearly gain information about the spatial distribution of vortices. Although not as spectacular as the electron-trapping method, the second-sound method provides more easily stable and reproducible measurements, at least in the present state of progress. Moreover, the second sound still appears to be the probe best suited to investigating states with a large number of vortices.

We report here accurate measurements of the variation of second-sound amplitude in a rotating cavity as a function of the angular velocity Ω (Sec. IV). Contrary to early experiments dealing with the spatial distribution of vortices,[2,4–7] where circular or annular containers have been used, we systematically experimented on rectangular cavities. At relatively high values of Ω, we also found that a narrow vortex-free region exists near the walls of the cavity. We confirm that the width of this vortex-free region, at equilibrium, is independent of the geometry of the boundaries as expected from theory (Sec. II). But what is to be emphasized in our results is the existence of metastable states in the whole explored

range of rotation velocities ($10^{-3} < \Omega/2\pi < 1$ rps). Metastability in rotating helium was sometimes observed,[2,3,5] sometimes not,[7] and reliable data do not exist in literature relating to this subject. The new important fact here is that the metastable states observed by slowly decreasing or increasing Ω are well-defined vortex states, quite reproducible and stable against small mechanical vibrations. Understanding the formation of such states ought to shed some light on the unsolved problem of how vortices appear and disappear in a rotating vessel.

Section II deals with the theory of stable and metastable equilibrium of vortices in cylindrical rotating containers of any arbitrary cross section. In particular, it is shown that the irrotational motion induced by the rotation of the walls (in noncircular cylinders) may be ignored in dealing with any equilibrium problem concerning vortices, such as determining, for instance, the value of the critical velocity Ω_c, the equilibrium positions of vortices, or the width d of the vortex-free region at high Ω.

In Sec. III, while describing the experimental arrangement, we detail the principle of using a second-sound wave to detect vortices. Any variation, due to rotation, of the second-sound amplitude in a rotating cavity will be conveniently expressed in terms of a variation of the total number of vortices N in the cavity, or more precisely of the weighted number $\bar{N}$ as defined in Sec. III.

The experimental results reported in Sec. IV suggest the existence of a free-energy barrier opposed to incoming or outgoing vortices. But the well-known barrier, as calculated from classical hydrodynamics following the same outlines as in Sec. II, obviously does not account for the metastable states observed. This point is discussed at the end of Sec. IV.

II. EQUILIBRIUM AND METASTABLE STATES IN A DEFORMED CYLINDER

We consider here the motion of He II in a cylindrical container of any cross section. The container rotates at angular velocity Ω about a vertical z axis parallel to the generators. Without loss of generality, the cylinder will be taken of unit thickness. The rotating helium is threaded by a system of vortices, which are supposed to behave like classical vortex lines, except that their circulation is quantized. The superfluid flow is regarded as the motion of an ideal incompressible fluid with density ρ_s. The two-dimensional motion of an incompressible fluid in a simply connected region R bounded externally by a rotating solid contour C, when a number of isolated vortices are present in the fluid, is a well-known problem in classical hydrodynamics.[8] This question, in connection with He II, has been studied in detail by Fetter.[9,10] So we recall briefly the basic formalism.

The superfluid velocity field $\vec{v}_s(\vec{r})$, and the corresponding stream function ψ, appear as the sum of two terms:

$$\vec{v}_s = \vec{v}_1 + \vec{v}_2, \quad \psi = \psi_1 + \psi_2 \ . \tag{1}$$

The first term $\vec{v}_1$ (or ψ_1) represents the irrotational flow arising from the rotation of the walls, whether or not vortices are present. ψ_1 is defined by the following condition:

$$\nabla^2\psi_1 = 0, \quad \psi_1 = \tfrac{1}{2}\Omega r^2 \ \text{ on } C \ . \tag{2}$$

The second term $\vec{v}_2$ is the velocity field induced by the vortices and their images. If N vortices are present at points $\vec{r}_i$, each having a quantum of circulation $\kappa = h/m$, ψ_2 is such that

$$\nabla^2\psi_2 = \sum_i \kappa\delta(\vec{r} - \vec{r}_i), \quad \psi_2 = 0 \ \text{ on } C \ , \tag{3}$$

and can be expressed as

$$\psi_2 = \sum_i \kappa G(\vec{r}\,|\,\vec{r}_i) = \sum_i \kappa\left[g(\vec{r}\,|\,\vec{r}_i) + \frac{1}{2\pi}\ln|\vec{r} - \vec{r}_i|\right] \ , \tag{4}$$

where G is the Green's function vanishing on C. The regular harmonic function $g(\vec{r}\,|\,\vec{r}_i)$ may be interpreted as that part of ψ_2 due to the images of the ith vortex.

Knowing ψ, the kinetic energy E and the angular momentum L of the superfluid are readily calculated:

$$E = \tfrac{1}{2}\rho_s \int (\vec{\nabla}\psi)^2 d^2r \ , \tag{5}$$

$$L = \rho_s \int (\vec{r}\cdot\vec{\nabla}\psi) d^2r \ . \tag{6}$$

Strictly, the integral (5) is divergent because of the logarithmic singularities of ψ_2 at the vortex cores $\vec{r}_i$. To exclude the singularities, we can draw small streamlines $\psi_2 = \text{const}$ around each vortex core, which are very like small circles c_i of radius a. Integrating over the multiply connected domain D bounded externally by C and internally by the small circles c_i, and since $\nabla^2\psi = 0$ in D, we obtain

$$E = \int_D (\vec{\nabla}\psi)^2 d^2r = \oint_{C+(c_i)} \psi \frac{\partial\psi}{\partial n} dl \ , \tag{7}$$

where $\vec{n}$ is the outward normal. Substituting the sum $\psi_1 + \psi_2$ for ψ, it follows from the properties (2) and (3) of ψ_1 and ψ_2 that the cross terms in Eq. (7) vanish. In other words, the kinetic energy E is the direct sum of the kinetic energies of each motion $\vec{v}_1$ and $\vec{v}_2$ considered independently. This result, unnoticed in Refs. 9 and 10, greatly simplifies further calculations.

At equilibrium, for a given Ω, both the number

and the positions $\vec{r}_i$ of the vortices are such as to minimize the kinetic "free energy" $F_s = E - L\Omega$.[9] From the additivity of the kinetic energies and angular momenta, it follows at once that F_s splits into two terms F_1 and F_2. The first term F_1, related to the irrotational motion $\vec{v}_1$, is a constant term. Therefore, the second term F_2 relating to the vortex field $\vec{v}_2$, must be minimum in the equilibrium state. According to Eqs. (3), (6), and (7), the free energy F_2 can be rewritten in terms of ψ_2 as

$$F_2 = E_2 - L_2\Omega = -\frac{\rho_s\kappa}{2}\sum_i \psi_2(c_i) + 2\Omega\rho_s\int \psi_2 d^2r \ . \tag{8}$$

Here, $\psi_2(c_i)$ is the constant value of ψ_2 on c_i at distance a of the vortex center $\vec{r}_i$:

$$\psi_2(c_i) \approx \sum_{k\neq i}\kappa G(\vec{r}_i|\vec{r}_k) + \kappa g(\vec{r}_i|\vec{r}_i) + \frac{\kappa}{2\pi}\ln a \ . \tag{9}$$

In Eq. (7) we have omitted the small model-dependent contributions of the cores. An effective core radius $a \sim 1-10$ Å can be defined in Eq. (9) precisely so as to include each core contribution in the term $\ln a$.

Tne Hamiltonian formalism, worked out by Hess[11] in the special case of circular geometry, can be extended to deformed cylinders. Let $\vec{v}_{si}$ be the superfluid velocity induced at the core of the ith vortex by the other vortices, including all the images, as well as by the irrotational flow $\vec{v}_1$. Denoting by prime symbols all quantities relative to the rotating frame of the container, the components of $\vec{v}'_{si}$ can be written as

$$\vec{v}'_{si} = \vec{v}_{si} - \vec{\Omega}\times\vec{r}_i \begin{cases} -\dfrac{\partial H}{\partial y_i'} \\ \\ \dfrac{\partial H}{\partial x_i'} \end{cases}, H = F_2/\rho_s\kappa. \tag{10}$$

Whether the number of vortices is fixed or not, the equilibrium requires F_2 to be stationary with respect to any displacement $\delta x_i'$, $\delta y_i'$ of the vortices. If so, Eq. (10) implies that v'_{si} must be zero, whence

$$\vec{v}_{si} = \vec{\Omega}\times\vec{r}_i = \vec{v}_n(\vec{r}_i) \quad \text{(equilibrium)}. \tag{11}$$

According to common ideas on mutual friction, it results from the condition (11) that the vortex line velocity $\vec{v}_{Li} = \vec{v}_{si}$. Thus, in equilibrium, the vortices follow the normal fluid and rotate rigidly with the container. As noted above, one may ignore the irrotational flow $\vec{v}_1$ when considering any question about the equilibrium of vortices, because of the additivity of the free energies F_1 and F_2. Nevertheless, some intricate relation must exist between the fields ψ_1 and ψ_2, evident in particular from Eq. (10), since, differentiating the function F_2, we obtain the total induced velocity $\vec{v}_{si}$, including $\vec{v}_1$.

When dealing with a large number of vortices, we may consider the vortex system as a continuous distribution with density $n(\vec{r})$. This continuum approximation becomes relevant when $nl^2 >> 1$, where l is a typical size of the container. We may introduce the averaged velocity field, $\langle\vec{v}_s\rangle = \vec{v}_1 + \langle\vec{v}_2\rangle$, and a stream function $\langle\psi_2\rangle$, which are related to $n(\vec{r})$ by

$$\begin{aligned} &\text{curl}\,\langle\vec{v}_s\rangle = \text{curl}\,\langle\vec{v}_2\rangle = n(\vec{r})\kappa = \nabla^2\langle\psi_2\rangle \ , \\ &\langle\psi_2\rangle = \kappa\int n(\vec{r})G(\vec{r}|\vec{r}')\,d^2r' \ , \end{aligned} \tag{12}$$

and Eq. (8) becomes

$$\begin{aligned} F_2 = &-\tfrac{1}{2}\rho_s\kappa^2\int\int n(\vec{r})n(\vec{r}')G(\vec{r}|\vec{r}')\,d^2r\,d^2r' \\ &+2\Omega\rho_s\int\int n(\vec{r})G(\vec{r}|\vec{r}')\,d^2r\,d^2r' \ . \end{aligned} \tag{13}$$

If the free energy F_2, as given by Eq. (13), is minimized with respect to the vortex density, it is found that $n(\vec{r}) = 2\Omega/\kappa = \text{const}$ throughout the whole region R. This is not surprising. It means that the liquid has a solid-body rotation, a well-known result for an ordinary fluid.[12] In Ref. 9, Fetter, using the total free energy $F_1 + F_2$, arrived at the same conclusion. Our purpose here is to reconsider the same variational calculus, but after correcting the expression (13), to allow for the discrete structure of the vorticity.

Equation (13) is strictly valid only for a vortex continuum, where the vorticity should be subdivided ad infinitum, that is in the limiting case where $\kappa\to 0$ and $n\to\infty$ (keeping $n\kappa$ constant). In the vortex continuum equivalent to the actual vortex distribution, suppose that a circular cell of radius b, carrying the vorticity κ, is replaced by a single quantized vortex at the center of the cell. An elementary calculation yields the resulting variation of the free energy:

$$\begin{aligned} \Delta F_2 &= \Delta E_2 - \Omega\Delta L_2 \\ &= \frac{\rho_s\kappa^2}{4\pi}\left[\ln\frac{b}{a} - \frac{1}{4} - \frac{\Omega}{\kappa}\pi b^2 + o(1)\right] \ . \end{aligned} \tag{14}$$

$b(\vec{r})$ is connected with the local vortex density by the obvious relation:

$$n\pi b^2 = 1 \ .$$

ΔF_2 represents the free-energy correction for one vortex located where the vortex density is $n(\vec{r})$. The same correction is repeated for each vortex. Thus we obtain a better continuum approximation for F_2 by including in Eq. (13) the following additional

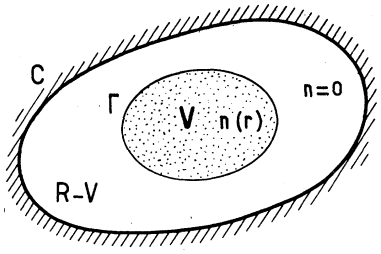

FIG. 1. Schematic of the model vortex distribution in an arbitrary cylinder viewed along rotation axis. The dotted region V bounded by the contour Γ represents the domain occupied by vortices with density $n(\vec{r})$. The annular region $R-V$ between the solid boundary C and the contour Γ is free of vortices.

term:

$$\int n(\vec{r})\Delta F_2(\vec{r})\,d^2r \ .$$

As suggested by experiments, let us now consider vortex states where only part V of the region R is occupied by vortices. The annular region $R-V$ surrounding the vortex domain is free of vortices. (See Fig. 1). Formulas (12) and (13) apply in this case by taking $n=0$ in the vortex-free region, while the condition $n >> l^{-2}$ still holds within the domain V. Thus we express that F_2 is stationary against any variation $\delta n(r)$ of the vortex density in V, subject to the condition that the total number of vortices remains constant:

$$N=\int_V n(r)\,d^2r=\text{const} \ . \tag{15}$$

This is equivalent to seeking an extremum, without constraint, of the function $F_2/\rho_s\kappa+\lambda N$, where λ is a constant Lagrange multiplier. Thus we get

$$-\kappa\int_V n(\vec{r}')G(\vec{r}|\vec{r}')\,d^2r'+2\Omega\int_R G(\vec{r}|\vec{r}')\,d^2r'$$
$$+\frac{\kappa}{4\pi}\left[\ln\left(\frac{b}{a}\right)-\frac{3}{4}\right]+\lambda=0 \quad (\text{for } \vec{r} \text{ in } V) \ . \tag{16}$$

Taking the Laplacian of both sides of Eq. (16), and disregarding fluctuations of $n(\vec{r})$ of wavelength comparable to the vortex spacing, as they are not physically significant in the continuum approximation, we deduce that

$$n(\vec{r})=2\Omega/\kappa=\text{const} \quad (\text{for } \vec{r} \text{ in } V) \ . \tag{17}$$

Equation (16) then reduces to

$$-2\Omega\int_{R-V}G(\vec{r}|\vec{r}')\,d^2r'=\frac{\kappa}{4\pi}\left[\ln\left(\frac{b}{a}\right)-\frac{3}{4}\right]+\lambda=\text{const}$$
$$(\text{for } \vec{r} \text{ in } V) \ . \tag{18}$$

The first condition (17) signifies that N vortices, wherever they are, must be uniformly distributed with the equilibrium density $n_0=2\Omega/\kappa$. This result already underlies the equilibrium requirement (11). If the induced superfluid velocity $\vec{v}_{si}$ and the mean velocity $\langle\vec{v}_s\rangle$ are identified as equal, Eq. (17) follows at once from Eqs. (11) and (12). With $n=n_0$ and $b^2=(n_0\pi)^{-1}$, the free-energy correction per vortex (14) can be rewritten as

$$\Delta F_2=\frac{\rho_s\kappa^2}{4\pi}\ln\left(\frac{b^*}{a}\right) \ ,$$
$$b^*=e^{-3/4}b=0.27s=0.27(\kappa/2\Omega)^{1/2} \ , \tag{19}$$

where $s=n_0^{-1/2}$ is the mean vortex spacing. This is exactly the correction derived by Tkachenko[13] for an infinite triangular lattice. As the free energy seems to be insensitive to the precise lattice structure,[14] this coincidence is not so surprising, and the isotropic cell model must be reasonably realistic.

The second condition (18) implicitly characterizes the domain V. The function of $\vec{r}$ in the left member of Eq. (18) may be interpreted as the superfluid stream function in the rotating frame, namely,

$$\langle\psi'\rangle=\psi_1+\langle\psi_2\rangle-\tfrac{1}{2}\Omega r^2 \ ,$$

and Eq. (18) states that $\langle\psi'\rangle$ has a constant value throughout the vortex domain. From this and from the general properties of ψ_1 and $\langle\psi_2\rangle$, it results that

$$\nabla^2\langle\psi'\rangle=\begin{cases}0 & (\text{in } V)\\ -2\Omega & (\text{in } R-V),\end{cases}$$
$$\langle\psi'\rangle=\begin{cases}0 & (\text{on } C)\\ \dfrac{\kappa}{4\pi}\ln\left(\dfrac{b^*}{a}\right)+\lambda & (\text{on and inside } \Gamma),\end{cases} \tag{20}$$

where Γ is the frontier of the domain V. In practical cases where the approximation holds, that is when $b << l$ (or $\Omega >> \kappa/l^2$), the vortex-free region is expected to be confined to a narrow strip along the boundary. Assuming that the radius of curvature of the boundary is large compared to the width d of the vortex-free strip, and using the above properties of $\langle\psi'\rangle$, we can write

$$\langle\psi'\rangle_C-\langle\psi'\rangle_\Gamma=-\langle\psi'\rangle_\Gamma\simeq-\Omega d^2 \ . \tag{21}$$

From Eqs. (20) and (21), we conclude that the vortex domain V must be such that the surrounding vortex-free strip is of constant width d, as given by

$$d^2=\frac{\kappa}{4\pi\Omega}\ln\left(\frac{b^*}{a}\right)+\frac{\lambda}{\Omega} \ . \tag{22}$$

If the constraint (15) is released, allowing the vortex number to vary, the calculations can be repeated by

simply setting $\lambda = 0$. The corresponding result refers to the thermodynamic equilibrium of the rotating system. In particular, the equilibrium vortex-free region should have the uniform width

$$d_0 = \frac{b}{\sqrt{2}}\left[\ln\left(\frac{b^*}{a}\right)\right]^{1/2} \quad \left(b^2 = \frac{\kappa}{2\pi\Omega}\right) , \tag{23}$$

which is independent of the shape of the boundary. Formula (23) has been proved[14] and experimentally tested[2,7] only for circular geometries, then presumed valid in more general cases.[14] Nevertheless, it was by no means obvious that the vortex-free strip should be of constant width in deformed cylinders. The irrotational flow $\bar{v}_1$, induced in this case by the rotating walls, is not of constant intensity along the boundary,[10] and so the flow $\bar{v}_1$, interfering with the vortex flow $\bar{v}_2$, could have altered the interaction between the vortices and their images, changing the width d accordingly.

Negative or positive values of the constant λ correspond to possible metastable states, that we shall refer to as N states, where the number of vortices N should be, respectively, larger ($d < d_0$) or smaller ($d > d_0$) than the equilibrium number N_0 ($d = d_0$). Metastable states are expected to arise if a free-energy barrier is opposed to incoming or outgoing vortices. In fact, a well-known consequence of the hydrodynamic equations is that a superfluid free-energy barrier should exist near the walls.[3,15] In the Appendix, we make use of the basic hydrodynamic relation (8) to calculate for an N state, the shape of the barrier opposed to an $(N+1)$th vortex. But, as we shall see in Sec. IV, this barrier model fails to explain our experimental results.

III. SECOND-SOUND METHOD AND EXPERIMENTAL PRINCIPLES

Except for the geometry of the resonator, the experimental arrangement is very similar to that described in a previous paper.[16] The cavities designed for the present work are parallelepipedic boxes machined from slabs of epoxy resine Araldite. They have a long rectangular cross section $l \times L$ as shown in Fig. 2. The representative data presented in Figs. 3–5 all refer to the same cavity; its dimensions are $l = 6$ mm, $L = 49$ mm, and $h = 23$ mm (vertical height). In Sec. IV, we shall refer to results obtained with four other resonators used, whose dimensions $l \times L \times h$ are as follows: $6 \times 23 \times 19$, $6 \times 54 \times 45$, $5 \times 46 \times 18$, and $3 \times 49 \times 23$ mm.[3] For the following discussion, we shall take the xy coordinate axes as indicated in Fig. 2, which are now to be viewed as fixed in the rotating frame.

A carbon transmitter painted on the wall of the cavity and heated by an ac current at frequency $\frac{1}{2}\omega$, generates a second-sound wave at frequency ω,

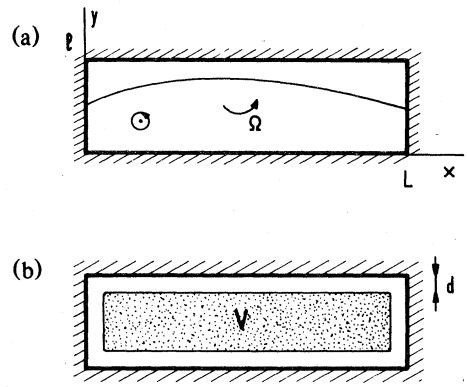

FIG. 2. (a) Cross-sectional sketch of a rectangular resonator driven at its fundamental x mode. A given vortex will contribute to damping according to its position along the velocity profile of the standing wave. In the weighted number of vortices $\bar{N}$ as defined in the text, a vortex at the antinode $x = \frac{1}{2}L$ is counted as 2, and a vortex near the nodes $x = 0$ and $x = L$ as zero. (b) At large angular velocities, vortices are expected to be uniformly distributed with density $2\Omega/\kappa$ up to a distance d from the walls. As compared to a cavity filled with vortices, the presence of the vortex-free region will have the effect of reducing the attenuation as though the mutual-friction parameter B were smaller by a factor $\gamma = 1 - 2d/L$.

$T_1(x,y,z)e^{-i\omega t}$. The temperature amplitude $T_1(x,y,z)$ can be expanded as a series of normal modes.[16] As ω is varied, the response of the cavity appears as a succession of resonant peaks. If ω approaches one of the eigenfrequencies, the corresponding resonant term predominates. Thus, one mode at a time can be observed, provided it is nondegenerate. For instance, suppose we are operating at the fundamental mode in the x direction or its mth harmonic:

$$T_1(x) = C_{m0}(\omega)\cos(m\pi x/L) , \tag{24}$$

by setting the driving frequency close to the characteristic frequency $\omega_{m0} = m\pi u_2/L$, where u_2 is the second-sound velocity. A receiving bolometer on the wall $x = 0$ (or $x = L$) measures both modulus and phase of the maximum temperature amplitude $T_1(0) = C_{m0}(\omega)$. The bolometric signal is fed into a lockin amplifier (LIA) PAR 129A. The two out-of-phase outputs of the LIA drive the two channels of an XY recorder, so that the complex amplitude T_1 is directly plotted on the Argand diagram.[16] When varying the exciting frequency ω, the response locus T_1 vs ω is a circle:

$$T_1(0) = C_{m0}(\omega) = A\left[1 + iQ\frac{\omega - \omega_{m0}}{\omega_{m0}}\right]^{-1} . \tag{25}$$

Here Q is the quality factor defined as the ratio of resonance frequency ω_{m0} to the half-width of the common response curve. The resonant amplitude A

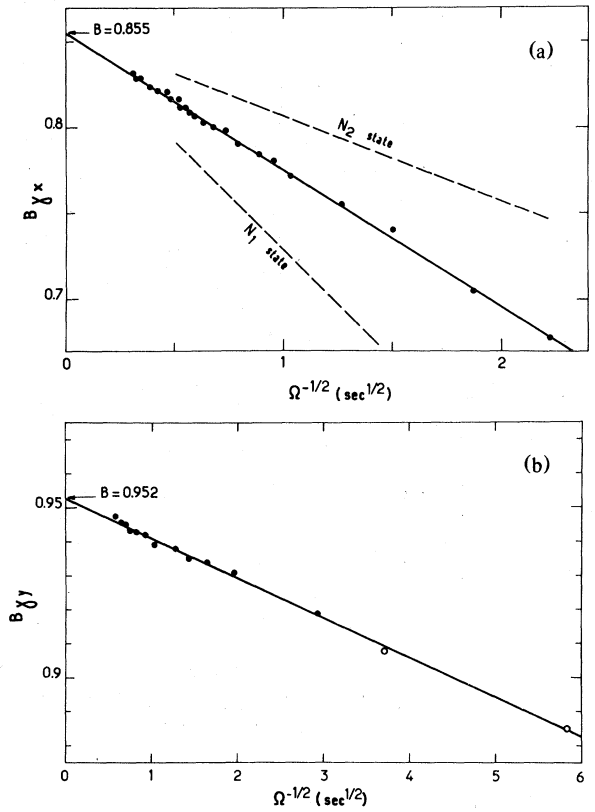

FIG. 3. Second-sound attenuation does not yield the mutual-friction parameter B directly, but instead the product $B\gamma$, where γ is a filling factor, depending on both the vortex state and the excited mode. γ would be unity, for all modes, if vortices filled the cavity. This figure shows data obtained at 1.9 K in the rectangular cavity $l \times L = 6 \times 49$ mm^2 as a function of the angular velocity Ω. (a) $B\gamma_x$ vs $\Omega^{-1/2}$, x fundamental mode (194 Hz), equilibrium state (solid circles). In nonequilibrium states, the variation domain of $B\gamma_x$ is bounded by the dashed lines, which correspond to the limiting N_1 and N_2 states. (b) $B\gamma_y$ vs $\Omega^{-1/2}$, y fundamental mode (1593 Hz), equilibrium state. The two last points (open circles) strictly speaking are beyond the domain of validity of the continuum approximation. Note that the extrapolated values of B are different in (a) and (b); this is related to the frequency dependence of B in accordance with the Hall-Vinen model (Ref. 17).

is related to Q by

$$A = (Z_\infty / m\pi)\bar{q}Q \ , \tag{26}$$

where Z_∞ is the characteristic impedance of helium, and $\bar{q}$ the averaged heat input, taking into account the geometry of the transmitter.[16] It should be recalled that the quality factor is a property of a given mode in a given cavity, and is independent of the location and size of the transmitter. Typically, in our experiments $\bar{q} \sim 10^{-4}$ mW/cm^2, $Q \sim 10^3$–10^4, $A \sim 10^{-5}$ K.

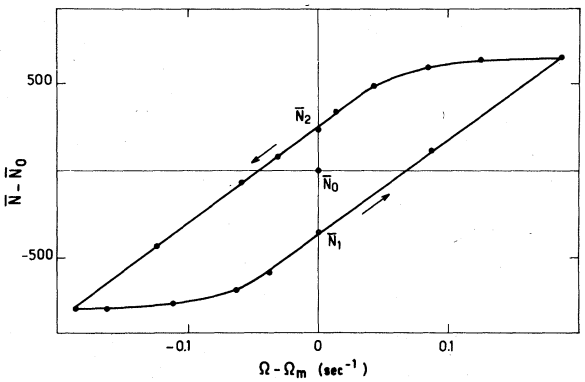

FIG. 4. Hysteresis loop showing the variation of the weighted vortex number, $\bar{N} = (2\Omega/\kappa)L/\gamma$, when quasistatically increasing then decreasing Ω around some mean value Ω_m ($T = 1.9$ K, $\Omega_m = 1.3$ sec^{-1}, cavity $l \times L = 6 \times 49$ mm,^{2} x fundamental mode). The equilibrium N_0 state, achieved after any strong perturbation, is taken as a reference state ($\bar{N}_0 = 6970$, $\gamma_x = 0.92$). Along the quasiparallel branches of the loop $\Delta\bar{N}$ is associated with a variation of the vortex density $2\Omega/\kappa$ ($\gamma \simeq$ const). At Ω_m, hysteresis variations $\bar{N}_1 - \bar{N}_0$, $\bar{N}_2 - \bar{N}_0$ are interpreted as variations of the width d of the vortex-free strip ($\gamma = 1 - 2d/l$): $d_1 = 0.39$, $d_0 = 0.25$, $d_2 = 0.15$ mm, for the N_1, N_0, and N_2 state, respectively.

Q^{-1} is proportional to the average dissipated power. In a nonrotating cavity, at working frequencies and temperatures, energy dissipation mainly arises from surface losses, owing to the friction of the normal fluid against the sides of the resonator. When rotating, each vortex present causes an additional dissipation through mutual friction. As the viscous penetration depth of the normal fluid is small compared to the width d of the vortex-free region, the two mechanisms of loss do not interfere. Thus, we may write

$$\frac{1}{Q} = \frac{1}{Q_0} + \frac{1}{Q_v} \ , \tag{27}$$

where Q_0 refers to the stationary resonator. Q_v is the quality factor which could result if the only source of damping was the mutual friction. According to the definition of the first mutual-friction parameter B (or strictly speaking of its real part B_1 (Ref. 17), the energy dissipation per unit time and per unit length of vortex line is

$$(\rho_n \rho_s / \rho)\tfrac{1}{2} B\kappa(\vec{v}_s - \vec{v}_n)^2.$$

ρ is the helium density, and $\rho_n = \rho - \rho_s$. Here, $\vec{v}_s - \vec{v}_n$ stands for the velocity field of the second-sound wave. Neglecting small quantities of the order of Ω/ω,[16] $\vec{v}_s - \vec{v}_n \propto \vec{\nabla} T_1$. A vortex contributes to energy dissipation according to its position in the standing wave. Vortices close to the walls $x = 0$ or L, which are nodes of the velocity field (for the con-

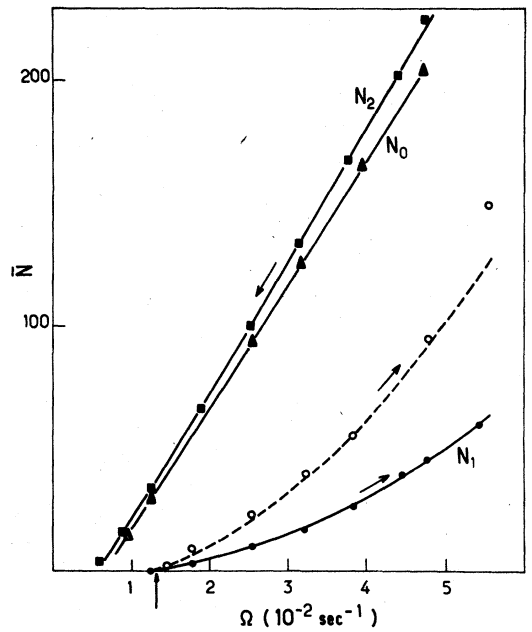

FIG. 5. Low-velocity results (cavity $l \times L = 6 \times 49$ mm,^{2} $T = 1.9$ K). $\bar{N}$ is given as a function of Ω for different vortex states and for both directions of propagation (fundamental modes). Circles, slowly increasing Ω: ●, $\bar{N}_1(x)$; ○, $\bar{N}_1(y)$. Squares, slowly decreasing Ω: ■, $\bar{N}_2(x)$. Triangles, equilibrium state: ▲, $\bar{N}_0(x)$. The $\bar{N}_2(y)$ and $\bar{N}_0(y)$ points, which mingle with the $\bar{N}_2(x)$ and $\bar{N}_0(x)$ points, are omitted for clarity. The lines are an aid to the eye; the dashed line is deduced from the lower full line by multiplication by a factor of 2. The arrow on the Ω axis shows the predicted value of the critical velocity Ω_c from Eq. (A5).

sidered modes), are undetected. For a system of N vortices located at points $\vec{r}_i(x_i,y_i)$, the quantity Q_v^{-1} can be written in the form

$$\frac{1}{Q_v} = \lambda B \kappa \sum_1^N \sin^2\left(\frac{m\pi x_i}{L}\right) , \tag{28}$$

where λ is a constant factor independent of the vortex properties. In the case of a large number of vortices uniformly distributed throughout the cavity, the sum in (28) is equal to $\frac{1}{2}N$. Assuming further the vortex density to be $n_0 = 2\Omega/\kappa$, and thus $N = n_0 Ll$, we must retrieve the known result derived from the hydrodynamic equations of rotating He II, namely, $Q_v = 2\omega/B\Omega$,[16] whence we obtain $\lambda = (2\omega Ll)^{-1}$. Equation (28) can then be rewritten as

$$\frac{1}{Q_v} = \frac{B\kappa}{2\omega Ll} \sum_1^N \sin^2\left(\frac{m\pi x_i}{L}\right) = \frac{B\kappa}{2\omega Ll}\frac{\bar{N}}{2} , \tag{29}$$

defining, for any vortex distribution, $\bar{N}$ as the number of vortices which, evenly distributed, would give rise to the same attenuation.

At large Ω, applying the continuum approximation, we have

$$\frac{1}{Q_v} = \frac{B\kappa}{2\omega Ll} \int_V n(\vec{r}) \sin^2\left(\frac{m\pi x}{L}\right) d^2r . \tag{30}$$

Since we are only considering states where the local equilibrium condition, $n = n_0$, holds, Eq. (30) may be put in the form

$$\frac{1}{Q_v} = \frac{B\Omega}{2\omega}\frac{2}{Ll} \int_V \sin^2\left(\frac{m\pi x}{L}\right) d^2r = \frac{B\Omega}{2\omega}\gamma , \tag{31}$$

where γ is a filling factor smaller than unity and related to $\bar{N}$ by

$$\gamma = \frac{\bar{N}}{n_0 Ll} = \frac{\kappa}{2\Omega Ll}\bar{N} . \tag{32}$$

In a metastable N state, as expected from theory (Sec. II), the vortex domain V is surrounded by a vortex-free strip of constant width d [Fig. 2(b)]. Then

$$\gamma_x \simeq 1 - 2d/l \quad (x \text{ modes}) . \tag{33}$$

The subscript x recalls that this value of γ is relative to any one of the modes (24). If, instead, the y fundamental mode or one of its harmonics was observed, we should have

$$\gamma_y \simeq 1 - 2d/L \quad (y \text{ modes}) . \tag{34}$$

One may ask whether the fluid flow near the sharp corners of the cavity is likely to give rise to any difficulties. Note that the arguments and results of Sec. II, up to and including Eq. (20), hold in a rectangular resonator. In particular, it should be emphasized again that the resulting superfluid flow $\vec{v}_1 + \vec{v}_2$ approaches solid-body rotation, so that, near the corners as well, the relative velocity $\vec{v}_s'$ remains very small ($v_s' \sim \Omega d$). Of course, Eq. (21) and comments about the constant width of the vortex-free strip do not apply near an angle, where the frontier Γ of the vortex domain, as defined by Eq. (20), is instead expected to be smoothly shaped. Corner effects can affect the vortex distribution over distances again of the order of d. But, whatever the resonant mode used, vortices near the corners will be undetected. So the detailed vortex distribution in the corners is clearly unimportant, and Eqs. (33) and (34) need no correcting.

The principle of the measurements is quite simple. The heat input $\bar{q}$ being maintained constant, changes in the resonant amplitude A connected to changes in the quality factor are measured. By comparing the amplitude in rotation $A(\Omega)$ with the rest amplitude $A(0)$, and knowing Q_0, Q_v can be calculated from the relation

$$\frac{1}{Q_v} = \frac{1}{Q_0}\left[\frac{A(0)}{A(\Omega)} - 1\right] . \tag{35}$$

Then Eq. (29) or Eq. (31) yields either the weighted vortex number $\bar{N}$ or the filling factor γ, which describe the spatial distribution of vortices in the cavity.

First of all, we check the perfect circular shape of the response curve, plotted in the complex plane as indicated above, ensuring that we actually observe a single mode and not some mixing of overlapping modes.[16] Q_0 is determined from the response curve of the stationary resonator. Then, setting the generator to the resonant frequency, the phase control of the LIA is adjusted for the X channel to be in phase with the resonant signal. A variation ΔX due to a change in the phase of the signal obviously should not be confused with a variation ΔA. Phase shifts may result from fluctuations of the driving frequency or of the bath temperature (because ω_{m0} as well as u_2 is temperature dependent). Although the phase can be checked on the Y channel, a strict control of both frequency and temperature is indispensable. The second-sound transmitter was driven by a very-low-frequency synthesizer ADRET 303, with frequency stabilization better than one part in 10^8. An auxiliary second-sound resonator of large Q was included in a feedback loop to control the temperature. This second-sound controller, that we have used previously,[16] has shown itself to be more efficient than a conventional bridge controller. Optimum performances are obtained about 1.9 K; without rotation, fluctuations are reduced to less than 10^{-8} K in the range 0–3 Hz, during 1 h. Moreover, in order that recorded variations $\Delta A/A$ as small as 5×10^{-4} be regarded as significant, we ascertained that the ac input power to the transmitter was stable during a run to better than 10^{-4}.

To increase the sensitivity of the method, it is clear from Eq. (35) that Q_0 should be as large as possible. The theoretical limit prescribed by surface losses can be approached, and values of Q_0 as large as 10 000 and greater are attainable if great care is used in the construction of the cavities. In the rectangular cavity 6×49 mm^2 mentioned above, we obtained, respectively, $Q_0=1250$ and 12 700 for the fundamental mode in the x direction and in the y direction.

IV. EXPERIMENTAL RESULTS AND DISCUSSION

As a preliminary remark, we will point out that, in the whole investigated range of angular velocities ($\Omega\sim10^{-2}$–10 sec^{-1}), the state of the rotating helium sample was found to be dependent on its past history. This was noted by other authors, using the electron-trapping method, in situations where the number of vortices is small ($N\sim1$–10).[3,5] We do, in fact, observe a well-marked metastability in the low-velocity range ($\Omega\lesssim10^{-1}$ sec^{-1}; Fig. 5), but we shall detect relative variations $\Delta N/N\lesssim10\%$ for angular velocities ranging from 1 to 10 sec^{-1} at which hysteresis phenomena are generally not reported.[7]

Figure 4 shows a typical recording of the small variations of the second-sound amplitude $A(\Omega)$ expressed in terms of $\Delta\bar{N}$, when slowly sweeping the angular velocity around some mean value Ω_m ($\Omega_m\pm\Delta\Omega$). We shall return below to the experimental conditions in which such a hysteresis loop can be observed. The state obtained at Ω_m by slowly increasing Ω, denoted as the N_1 state in the figure, is clearly distinct from the N_2 state obtained by decreasing Ω. In the N_2 state, there are about 600 more "averaged" vortices than in the N_1 state, N_1 and N_2 being of the order of 7000 (at $\Omega_m=1.3$ sec^{-1}). If, on the contrary, the rotation is rapidly set to Ω_m, either starting from zero or from some high value above Ω_m, we obtained an intermediate state, marked as N_0 in Fig. 4, which we have reason to identify with the state of thermodynamic equilibrium. As a matter of fact, this N_0 state inevitably occurs after any strong perturbation of the rotating system. Whatever the initial state may be, jarring the cryostat brings the system by steps to the N_0 state. The same result is obtained by momentarily feeding a large dc heat flux into the cavity.

Equilibrium states (high-velocity range)

In reproducing systematically the N_0 state, thus defined experimentally, we first investigated the variations of the second-sound amplitude $A(\Omega)$ as a function of the angular velocity for relatively large values of Ω ranging from 10^{-1} to 10 sec^{-1}. In this range the continuum approximation holds, i.e., $b\ll l\sim1$ cm, or equivalently $\Omega\gg\kappa/l^2\sim\Omega_c$. Taking for granted that $n=2\Omega/\kappa$ in the vortex domain, we can calculate the filling factor γ from the experimental data using Eqs. (31) and (35), provided that B is known. But B itself has to be deduced from such amplitude measurements. In fact, what is precisely measured as a function of Ω is the global quantity $B\gamma$ appearing in Eq. (31). Theoretically, γ should be given by Eq. (33) or (34) according to the excited mode, substituting, for equilibrium, $d=d_0$ as given by Eq. (23). The logarithmic factor in Eq. (23) only varies by a few percent in the interval of angular velocities studied, so that it may be approximately regarded as constant, and $d_0\propto\Omega^{-1/2}$. Thus we expect $B\gamma$ has the simple dependence:

$$B\gamma_{x/y}=B(1-c_{x/y}\Omega^{-1/2}) \quad . \tag{36}$$

This approximate formula well accounts for the experimental results. Figure 3 shows experimental values of $B\gamma_x$ and $B\gamma_y$ obtained at 1.9 K in the 6×49 mm^2 cavity. For the fundamental x mode ($\omega_{10}/2\pi=194$ Hz) the data $B\gamma_x$ vs $\Omega^{-1/2}$ are well fit-

ted by the straight line:

$$B\gamma_x = 0.855(1 - 0.093\Omega^{-1/2}) \ , \tag{37}$$

while for the y fundamental mode ($\omega_{01}/2\pi = 1593$ Hz) the best fit is

$$B\gamma_y = 0.952(1 - 0.012\Omega^{-1/2}) \ . \tag{38}$$

We immediately note the difference between the two values of B in (37) and (38), which must be attributed to the dependence of B on the sound frequency in accordance with the Hall-Vinen model, as shown by Mehl.[17] Such an effect cannot be ignored in our experiments. Taking B as a constant in Eq. (31) would alter our conclusions on the spatial distribution of vortices. Conversely, the correcting factor γ should be taken into consideration, when determining this slight dependence of B on ω; our own results on this question will be published elsewhere.

While B is determined to better than 1%, the slopes of the fitting lines, i.e., c_x and c_y, cannot be given to better than a few percent. The experimental ratio $c_y/c_x = 0.13$, as deduced from Eqs. (37) and (38), is close to the predicted value $c_y/c_x = l/L = 0.122$ within better than 10%. This confirms that the vortex-free strip has the same width along the small and the large sides of the cavity. By measuring the attenuation of the third and fifth harmonics ω_{30} and ω_{50} we detected no change in c_x within the accuracy of measurments, indicating that the vortex-free strip is of uniform width d along the large sides L. From the study of four cavities of different dimensions l and L (6×49, 6×23, 5×46, 3×49 mm^2), it appears again that c is proportional to L^{-1} or l^{-1}. All these results corroborate the existence, at equilibrium, of a vortex-free strip having a constant width d_0 independent of the shape and size of the container.

As said above, the logarithmic factor $(\ln b^*/a)^{1/2}$ involved in the expression of d_0 or c has a variation of a few percent over the experimental velocity range. For example, assuming $a = 10$ Å, the mean of the extremal values of this factor is 3.27 in Fig. 3(a), and 3.39 in Fig. 3(b). Whence we obtain the theoretical values $c_x = 0.097$, $c_y = 0.012$, in fair agreement with the experimental ones in (37) and (38). Changing a by a factor 2 affects c_x and c_y by $\pm 3\%$, so we may only hope to get an order of magnitude of the effective core radius a. Although a may be chosen to fit the experimental data (provided that $c_x/c_y = L/l$), the fact remains that for plausible values of a from 1 to 100 Å, d_0 or c_x, c_y remain within a narrow range. Consequently, it can be stated that, not only its variation as $\Omega^{-1/2}$ but also the predicted value of d_0 have proven correct. In passing, we may wonder at the success of a continuum model, when d_0 is comparable to the vortex spacing.

If, instead of looking at the so-called N_0 states, we had systematically used, for instance, the data relative to the metastable N_1 or N_2 states, we should have obtained lines $B\gamma_x$ vs $\Omega^{-1/2}$ [dashed lines in Fig. 3(a)] well apart from the N_0 line. While the extrapolated value of B would be the same, the corresponding values of c_x would be quite different. To account for these slopes through the formula $c_x\Omega^{-1/2} = 2d_0/l$ we should have to allow for absurd values of a such as 10^{-4} or 10^4 Å. This gives another argument in favor of the N_0 state being actually the thermodynamic equilibrium state.

Having determined B (at a given frequency ω) from high-velocity results, all amplitudes measured, at any Ω (Figs. 4 and 5), can be expressed in terms of the weighted number of vortices $\bar{N}$, as defined by Eq. (29). When necessary, the direction of propagation will be specified by noting $\bar{N}(x)$ or $\bar{N}(y)$.

Metastable states

Let us now specify the experimental conditions for observing a hysteresis loop such as shown in Fig. 4:

(i) The loop is obtained by points by slowly increasing and decreasing Ω from one point to the next, and waiting for (metastable) equilibrium at each point. This loop is unchanged as long as the angular acceleration lies below some critical threshold. So it represents a quasistatic cyclic process of the rotating system. The loop in Fig. 4 was observed when $|d\Omega/dt| < 10^{-4}$ sec^{-2}, corresponding to a total run time greater than 2 h. If $|d\Omega/dt|$ rose above this critical value, the loop shrank. At the other extreme, when the angular velocity Ω_m was reached after large angular accelerations, the system systematically comes to the N_0 state, taken as reference state in Fig. 4.

(ii) Too large a dc heat flux fed into the cavity also makes the loop shrink. But a dc heat flux necessarily accompanies the ac heat flux from the second-sound transmitter. For the vortex state to be unaffected, we were forced to operate with an ac input power $q \lesssim 0.2$ mW/cm^2. This may explain why hysteresis phenomena can escape detection in second-sound experiments.[7]

(iii) The values $\bar{N}_1$ and $\bar{N}_2$ measured at the mean angular velocity Ω_m are independent of the sweep amplitude $\pm\Delta\Omega$, provided that $\Delta\Omega$ is not too small (in Fig. 4, $\Delta\Omega \gtrsim 0.1$ sec^{-1}).

Thus for each value of the angular velocity we experimentally define three vortex states perfectly reproducible within the accuracy of measurments: the N_0 state observed after any strong perturbation of the system, which we have interpreted as the thermodynamic equilibrium state; then the metastable N_1 and N_2 states obtained when respectively increasing and decreasing Ω quasistatically. If the rotational velocity has been settled following any process, we may obtain any intermediate metastable state

between the N_1 state and the N_2 state, i.e., $\bar{N}_1 < \bar{N} < \bar{N}_2$. We never observed that $\bar{N} > \bar{N}_2$ or $\bar{N} < \bar{N}_1$.

The reproducibility of the two limiting states $\bar{N}_1$ and $\bar{N}_2$ allows us to test the conclusions of Sec. II concerning the metastable states in the high velocity range. A variation of the vortex number around N_0 should result in a variation around d_0 of the still uniform width d of the vortex-free strip. Let $d = d_1$ and d_2 in the N_1 and N_2 state, respectively. According to Eqs. (32), (33), and (34), we thus expect that

$$\bar{N}_2(x) - \bar{N}_1(x) = \frac{4\Omega}{\kappa} L (d_1 - d_2) = \frac{L}{l} [\bar{N}_2(y) - \bar{N}_1(y)] \ . \quad (39)$$

In the conditions of Fig. 4, by exciting the fundamental mode ω_{10} we found $\bar{N}_2(x) - \bar{N}_1(x) = 590 \pm 20$. Within this accuracy, the harmonics ω_{30} ω_{50} yield the same result, as it should be. In the y direction, we expect from (39) a hysteresis effect $\Delta\bar{N} = \frac{6}{49} \times 590 = 72$ "averaged" vortices; experimentally we found $\bar{N}_2(y) - \bar{N}_1(y) = 70 \pm 5$, bearing out that the vortex-free strip has the same extent all round the walls as in the equilibrium state.

Incidentally, we infer from these results that the pinning of vortex lines, if it exists, does not prevent N vortices (N being fixed) from finding their equilibrium distribution.

Surface irregularities were introduced on the horizontal faces of the 6×49 mm^2 cavity to enhance the pinning. Each horizontal face was spotted throughout with specks of silver paint, forming asperities of the order of 0.1 mm. No resulting change in the hysteresis loop of Fig. 4 was observed. We have not tried testing vertical faces similarly, since a large part of them was occupied by transmitting and receiving films.

All measurements obtained with diversely dimensioned resonators (dimensions quoted at the beginning of Sec. II) consistently show that d_1 and d_2 are independent of the cavity dimensions, including its vertical height. At a given temperature, the hysteresis difference $d_1 - d_2$ only depends on the angular velocity. At 1.9 K, our results in the range 10^{-1} to 10 sec^{-1} are well fitted by the empirical law.

$$d_1 - d_2 \simeq 0.26 \Omega^{-1/2} (\text{mm}) \quad (T = 1.9 \text{ K}) \quad (40)$$

The question is now what restricts the variation interval (N_1, N_2) of the vortex number. At a given Ω, N_1 and N_2 are, respectively, the minimum and maximum observable. We wish to emphasize that the N_1 and N_2 states are well-defined states, recoverable from day to day. We could verify the stability of any metastable state along the cyclic process of Fig. 4 during periods larger than 2 h. Only strong perturbations were able to alter the vortex state.

Free-energy barrier

These features strongly suggest the existence of a free-energy barrier for vortices entering or leaving the cavity. To be consistent with experiment, the barrier height should vanish for outgoing vortices when $N \geqslant N_2$, and for incoming vortices when $N \leqslant N_1$. As a matter of fact, a well-known consequence of the hydrodynamic model is that an energy barrier should exist next to the boundary, whether the cavity is free of vortices or not (see Appendix). The calculated free-energy profile $\Delta F_s(y)$ associated with the appearance of an $(N+1)$th vortex at distance y from the wall, changes shape as N is increased from zero, as shown in Fig. 6. From Eqs. (A4) or (A7) it is seen that a strong barrier $\Delta F_s(y_m) \sim 10^8 k_B T$ cm^{-1} is always opposed to incoming vortices, except perhaps at extremely high $\Omega \sim 10^4$ sec^{-1}, so that in any practical case N_1 ought to be zero. Moreover, the same calculation predicts that the outgoing barrier disappears for N exceeding some value $N_2 > N_0$ ($d_2 < d_0$). For example, at $\Omega = 1.3$ sec^{-1} we found $d_2 = 0.11$ mm (curve III in Fig. 6), roughly agreeing with the experimental value $d_2 = 0.15 \pm 0.01$ ($\gamma_x = 0.95$ for the N_2 state in Fig. 4). Concerning d_2, we did not expect a better estimate, not so much because the N state is regarded as a vortex continuum, as because it is supposed to be unperturbed as y tends to d. Yet we can hardly consider this quasiagreement as significant, since, on the other hand, the same model fails to explain the

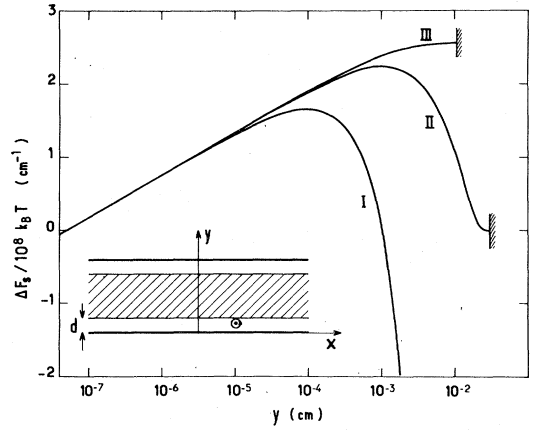

FIG. 6. Calculated free-energy barrier $\Delta F_s(y)$ associated with the entrance of an $(N+1)$th vortex according to Eqs. (A4) and (A7), taking $l = 6$ mm, $\rho_s = 0.083$ g cm^{-3} (1.9 K), $a = 10$ Å. Curve I: penetration of a first vortex ($N = 0$). Curve II: vortex state near equilibrium; $d = 0.29$ mm ($\simeq d_0$) in Eq. (A7). Curve III: vanishing barrier energy for outgoing vortices; $d = d_2 = 0.11$ mm. These curves lose their meaning when y approaches the core radius a. On the other hand, the vortex domain has been assumed to be unperturbed, making the curves II and III unrealistic when y tends to d.

observed N_1 state. For the sake of simplicity we have made the usual assumption that vortices remain straight and penetrate by a simple lateral displacement. The vortices are more likely to enter the fluid in a complicated manner, for instance, by progressively growing from a first-line element. This is supported by the fact that the hysteresis amplitude $d_1 - d_2$ is found to be independent of the vertical dimension of the rotating cavity. However, if we think of a first vortex element as having a vertical height comparable with the barrier thickness, i.e., about a few micrometers, the effective barrier height would be still of the order of $10^4 k_B T$. Clearly vortices cannot overcome the barrier by thermal fluctuations.

To explain that, in spite of this barrier, vortices actually enter the fluid, it is generally believed that random mechanical vibrations supply the necessary energy.[15] Indeed, strong mechanical disturbances bring the system to the N_0 state. So, it may be argued that the ambient vibrations, unable though they are to achieve the N_0 state, cause the vortices to enter up to some filling level corresponding to the N_1 state. But this argument is incompatible with the fact the N_1 and N_2 states are quite reproducible states which are stable against small mechanical vibrations. Furthermore, improvements in the elements of the speed control system or transmission coupling (electronics, servomotor, flywheel, ball-bearings) have reduced the small spurious accelerations of the rotating apparatus, but no change in the positions of the N_1 and N_2 states was observed. Furthermore, artificially enhanced floor vibrations did not alter the results either. Therefore, we are brought back to the conclusion that the occurrence of limiting states N_1 and N_2 is connected to some fundamental effect such as the existence of a free-energy barrier, whose correct analysis ought to lead to simple laws such as Eq. (40).

The hydrodynamic model and experimental facts might perhaps be reconciled in two ways, on which we shall briefly comment. By assuming that the free-energy barrier reduces to the superfluid barrier $\Delta F_s(y)$, we have implicitly allowed only for perturbations of the superfluid velocity field. Now, a vortex penetrating along a real path necessarily has a line velocity $\vec{v}_L \neq \vec{\Omega} \times \vec{r}$ and consequently drags the normal fluid in its vicinity. Any change in the normal velocity field is a perturbation of the equilibrium distribution $\vec{v}_n = \vec{\Omega} \times \vec{r}$, involving an increase in the normal free energy F_n, so that the effective barrier should be the total free-energy barrier $\Delta F_n + \Delta F_s \geq \Delta F_s$. At the maximum y_m of the superfluid barrier the induced velocity $\vec{v}_s$ is precisely equal to $\vec{\Omega} \times \vec{r}$ according to Eq. (10), so that $\vec{v}_L = \vec{\Omega} \times \vec{r}$ and $\Delta F_n = 0$. On the contrary, for a vortex next to the wall, v_s, and hence v_L, is very large compared with Ωr because of the proximity of the image vortex. In this region (say, $y \gtrsim 10a$) a rough estimate of ΔF_n will be inferred by adopting the naive model of a solid wire moving with a velocity $\vec{v}_L$ and dragging an ordinary fluid otherwise at rest. Let us refer to the relevant classical problem of the low-Reynolds-number flow past a cylinder[18]: The normal fluid, with a viscosity μ, is dragged over distances from the core of the order of $\delta = \mu/\rho_n v_L$, and the resulting increase in free energy is $\Delta F_n \sim \rho_n v_L^2 \delta^2 = \mu^2/\rho_n \sim 10^8 k_B T$ cm.$^{-1}$ It would be a considerable task to calculate the exact shape of the barrier $\Delta F_s + \Delta F_n$, but the effect of the additional term ΔF_n is clearly to broaden the barrier and possibly level up the free-energy profile, so that a vortex produced at the wall should not be driven back. Of course, the barrier has not disappeared, but it has shifted closer to the wall at a distance comparable to the core radius. If so, approximately the same energy per unit length must be supplied for a vortex to be created, but this energy should be supplied in the process of vortex formation at the wall, thermal fluctuations now playing a dominant role. Nevertheless, if we persist in considering F_s as the effective potential, another imaginable process may be a collective penetration of a vortex bundle, taking advantage of the interaction free energy stored during the formation—a possible event—of such a bundle on the wall. Anyway, we are faced, beyond the field of hydrodynamics, with the difficult problem of vortex nucleation and formation of preexisting vortices on the wall. Still the above arguments may remain unconvincing and, in a sense, this discussion rather reveals the inadequacy of the semiclassical model of vortex lines, when dealing with surface-barrier phenomena.

Low-velocity range

We shall end this discussion by some comments on the results obtained in the low-velocity range ($\Omega < 10^{-1}$ sec^{-1}, Fig. 5). When dealing with a small number of vortices, the quantity $\bar{N}$, unlike γ, remains meaningful and follows at once from amplitude measurements through Eqs. (29) and (35). Recall that $\bar{N}$ vortices evenly distributed throughout the cavity would give the same attenuation as that actually observed. For a given vortex state, $\bar{N}$ depends on the mode used to probe the vortex distribution.

The N_1 states (lower lines in Fig. 5) are reached by quasistatically increasing Ω from zero ($d\Omega/dt \lesssim 10^{-5}$ sec^{-2}). The N_2 curve (upper line in Fig. 5) is described by starting from high velocities, then slowly decreasing Ω down to zero. We retrieved all the features stated above: stability and reproducibility of the N_0, N_1, and N_2 states, and also the limiting property, i.e., $\bar{N}_1 < \bar{N} < \bar{N}_2$, whatever the past history of the helium sample may be. However, it is to be noted that in the low-velocity range, the equilibrium N_0 state is comparitively much closer to the N_2 state.

The pronounced hysteresis of the N_1 state is compatible with recent results by electron trapping.[5]

Up to $\Omega \simeq 5 \times 10^{-2}$ sec^{-1}, we note a factor of 2 between the values of $\bar{N}_1$ when observed in the two directions of propagation. This is most simply interpreted by granting that the vortices in the N_1 state are evenly distributed on the median line of the cavity, $y = \frac{1}{2}l$. N_1 being the true number of vortices, we thus have

$$\bar{N}_1(x) \simeq N_1, \quad \bar{N}_1(y) = 2N_1 \quad (\Omega \lesssim 5 \times 10^{-2} \text{ sec}^{-1}) \ .$$

This clearly shows that, even in situations where vortices have become scarce, the prevailing factor in determining their spatial distribution still remains the interaction between vortices and their images. Neither pinning effects nor fluctuations can blur the vortex pattern of minimum free energy (N being fixed).[5] In contradistinction to $\bar{N}_1$, no significant difference was detected between $\bar{N}_2(x)$ and $\bar{N}_2(y)$, neither between $\bar{N}_0(x)$ and $\bar{N}_0(y)$. This suggests that vortices in the N_0 and N_2 states keep spreading throughout the cavity down to the lowest worked velocities.

When Ω was decreased to zero, we were unable to detect a single vortex line, and we never observed any steplike variation of $\bar{N}$ associated with the discrete nature of the vorticity. Nevertheless, the sensitivity at very slow rotation could attain three to five vortices, permitting a good determination of the critical velocity Ω_c in extrapolating the N_0 curve. For the rectangular cavity 6×49 mm,[2] we find from Fig. 5, $\Omega_c(\text{expt.}) = 6.0 \pm 0.6 \times 10^{-3}$ sec.$^{-1}$ To compare with the theoretical value, we may use Eq. (A5) which gives the correct result to better than 0.5% as soon as $L/l > 4$.[10] Substituting $l = 6$ mm, $a \sim 10$ Å, we obtain $\Omega_c(\text{theory}) = 13 \times 10^{-3}$ sec^{-1}, which is more than twice the experimental value. The fact that $\Omega_c(\text{theory})$ roughly corresponds to the beginning of the N_1 curve is no doubt a pure coincidence, which should not obscure this discordance between theory and experiment. In other words, referring to Fig. 5, let us suppose we set $\Omega = 10^{-2}$ sec^{-1}, for instance. At such an angular velocity thermodynamics unambiguously indicate that the irrotational motion ($N = 0$) should be the state of minimum free energy, and yet we observe that the most stable state contains about 20 vortices. We have no explanation for this discrepancy that we have clearly retrieved from run to run. Results obtained with other available resonators seem to indicate that Ω_c decreases with increasing l more rapidly than l^{-2}. For instance, in the cavity 3×49 mm,[2] we found $\Omega_c(\text{expt}) = 34 \pm 2 \times 10^{-3}$ sec^{-1}, to be compared with $\Omega_c(\text{theory}) = 51 \times 10^{-3}$ sec^{-1}. Further experiments are required to clear up this point.

Summary

In the high-velocity range ($\Omega >> \Omega_c$), where the vortex state may be regarded as a continuum, we have shown, both by theory and experiment, that, independently of the geometry of the boundaries:

(i) The equilibrium state of a given number N of vortices appears as a uniform distribution leaving along the walls a narrow vortex-free strip of constant thickness d (Fig. 2).

(ii) in the thermodynamic equilibrium (N unconstrained), $d = d_0$ in accordance with Eq. (23).

In circular cylinders, whereas the first point obviously follows from symmetry, the second point was established theoretically by Stauffer and Fetter,[14] and experimentally in an annulus by Shenk and Mehl.[7] Note, however, that the condition $\Omega >> \Omega_c$ was not satisfied for most of the data used in Ref. 7 to test the theoretical expression of d_0. On the other hand, Northby and Donnelly,[2] working with an annulus at angular velocities well above Ω_c, had measured a vortex-free thickness about double the predicted value.

In the low-velocity range, we pointed out that the critical angular velocity Ω_c was found to be roughly half the theoretical value. This disagreement with theory cannot be resolved by a reasonable choice for the core radius parameter a.

In the whole range of angular velocities, we have demonstrated the existence of two limiting metastable states, we have called the N_1 and N_2 states. The observed number of vortices, at a given Ω, is history dependent, but lies between two experimentally well-defined values N_1 and N_2, which are unaffected by mechanical vibrations. At high Ω, N_1 and N_2 correspond to extremal values d_1 and d_2 of the vortex-free thickness. Like d_0, d_1 and d_2 are independent of the shape of the boundaries. Hysteresis indicates the presence of some barrier energy. Considering the possible role of mechanical vibrations, the hydrodynamic barrier energy might explain that N varies throughout a somewhat undefined interval, depending on the vibration level in the apparatus. However, the existence of definite limits N_1 and N_2 contradicts this scheme. The present data may be useful in reexamining the barrier-energy problem on quantitative grounds.

From all these experiments, we are tempted to conclude that the semiclassical model of vortex lines leads to correct quantitative results as far as vortex states with a large number of vortices are concerned. But, for undetermined reasons, this model fails to explain processes involving a single vortex or a few vortices, such as the processes of appearance and disappearance of vortices (barrier problem) and the formation of the first vortex states in the low-velocity range (Ω_c problem).

APPENDIX

When a vortex moves from the walls of the cavity into the fluid, it must overcome a superfluid free-energy barrier $\Delta F_s(\vec{r})$, whether vortices are already present in the cavity or not. In this appendix, the classical hydrodynamic model of Sec. II is used to derive the shape of this barrier.

Let $F_s(N)$ be the superfluid free energy of the rotating system for an N state, that is a metastable equilibrium state with N vortices such as described in Sec. II. Starting from an N state, suppose an additional vortex to be located at $\vec{r}$ in the vortex-free region $R-V$. So, we obtain a second state, the free energy of which is denoted by $F_s(N,\vec{r})$. Again, the constant term F_1 may be omitted, so that $\Delta F_s(r)$ is equal to the corresponding change in the free energy F_2. Making use of Eqs. (4) and (8) we find that

$$\Delta F_s(\vec{r}) = F_2(N,\vec{r}) - F_2(N) \tag{A1}$$
$$= -\rho_s\kappa\psi_2(\vec{r}) + F_2(0,\vec{r}) \ .$$

Here ψ_2 is the stream function solely due to the N vortices in the domain V. The last term $F_2(0,\vec{r})$ is just the barrier opposed to a first penetrating vortex $(N=0)$ and can be written as

$$F_2(0,\vec{r}) = -\frac{\rho_s\kappa^2}{2}\left[g(\vec{r}\,|\,\vec{r}) + \frac{1}{2\pi}\ln a\right]$$
$$+2\Omega\rho_s\kappa\int_R G(\vec{r}\,|\,\vec{r}\,')d^2r' \ . \tag{A2}$$

The integral in Eq. (A2) is the function $f(\vec{r})$ which solves the equation $\nabla^2 f = 1$ and vanishes on the boundary C.

Now, as a simple application, let us consider the limiting case of a parallel-plate cavity which approximates the long rectangular resonators we used in our experiments. Taking the walls as the planes $y=0$ and $y=l$, a straightforward calculation yields

$$g(\vec{r}\,|\,\vec{r}) = -\frac{1}{2\pi}\ln\left[\frac{2l}{\pi}\sin(\pi y/l)\right] \ , \tag{A3}$$
$$f(\vec{r}) = \tfrac{1}{2}y(y-l) \qquad (0<y<l) \ ,$$

whence

$$F_2(0,\vec{r}) = \frac{\rho_s\kappa^2}{4\pi}\ln\left[\frac{2l}{\pi a}\sin\left(\frac{\pi y}{l}\right)\right] + \rho_s\kappa\Omega y(y-l) \ . \tag{A4}$$

$F_2(0,\vec{r})$ has a minimum at $y=\frac{1}{2}l$. As Ω is raised from zero, the value of $F_2(0,\vec{r})$ at the central minimum decreases, and becomes negative above some critical velocity Ω_c. For Ω_c, it becomes thermodynamically favorable to introduce vortices midway between the walls. Below Ω_c the purely irrotational motion is the preferred state. Ω_c is determined by expressing that $F_2(0,\vec{r})=0$ at $y=\frac{1}{2}l$:

$$\Omega_c = \frac{\kappa}{\pi l^2}\ln\left(\frac{2l}{\pi a}\right) \ . \tag{A5}$$

Figure 6 (curve I) shows a plot of $F_2(0,\vec{r})$ near the wall $y=0$, for some value of Ω large compared with Ω_c ($\Omega/2\pi = 0.2$ sec^{-1}, $l=6$ mm, $a=10$ Å). Typically, for $\Omega\sim 1$, $F_2(0,\vec{r})$ has a maximum at a distance of about 1 μm from the wall. Although vortex-free states are never observed in this range of angular velocities, it is interesting to note that the height of the free-energy barrier for a first penetrating vortex would be still of the order of $10^8 k_B T$ cm^{-1}.

Consider at large angular velocity ($\Omega \gg \Omega_c$) an N state near the equilibrium state ($N\sim N_0$). Vortices are uniformly distributed with density $n_0 = 2\Omega/\kappa$ except in two narrow strips of width d along the walls. The resulting ψ_2 is readily expressed by means of linear and quadratic functions. For instance, let there be a $(N+1)$th vortex near the wall $y=0$. To calculate $\Delta F_s(\vec{r})$ according to (A1) we need to explicit ψ_2 in the region $y<d$:

$$\psi_2 = -\Omega(l-2d)y \qquad (0<y<d) \ . \tag{A6}$$

Then assuming $d \ll l$ we obtain from Eqs. (A1), (A4), and (A6)

$$\Delta F_s(\vec{r}) = \frac{\rho_s\kappa^2}{4\pi}\ln\left(\frac{2y}{a}\right)$$
$$+\rho_s\kappa\Omega(y-2d)y \quad (0<y<d) \ . \tag{A7}$$

Note that the barrier profile no longer depends on l. Insofar as d is small compared with the dimensions of the container, the last expression (A7) is certainly valid for any shape of the boundary, y standing in any case for the distance from the additional vortex to the wall.

The barrier profile (A7) is shown in Fig. 6, for $d=d_0$, i.e., at thermodynamic equilibrium (curve II), and for the value d_2 ($d_2<d_0$) at which the maximum of the barrier disappears (curve III).

[1]I. M. Khalatnikov, *Introduction to the Theory of Superfluidity* (Benjamin, New York, 1965), Chap. 16.
[2]J. A. Northby and R. J. Donnelly, Phys. Rev. Lett. 25, 214 (1970).
[3]R. E. Packard and T. M. Sanders, Jr., Phys. Rev. A 6, 799 (1972).
[4]G. A. Williams and R. E. Packard, Phys. Rev. Lett. 33, 280 (1974).
[5]M. J. V. Gordon, G. A. Williams, and R. E. Packard, J. Phys. (Paris) 39, C6-172 (1978); E. J. Yarmchuk, M. J. V. Gordon, and R. E. Packard, Phys. Rev. Lett. 43, 214 (1979).
[6]P. J. Bendt and R. J. Donnelly, Phys. Rev. Lett. 19, 214 (1967).
[7]D. S. Shenk and J. B. Mehl, Phys. Rev. Lett. 27, 1703 (1971).
[8]C. C. Lin, Proc. Nat. Acad. Sci. U.S.A. 27, 570 (1941); 27, 575 (1941).
[9]A. L. Fetter, Phys. Rev. 152, 183 (1966).
[10]A. L. Fetter, J. Low. Temp. Phys. 16, 533 (1974).
[11]G. B. Hess, Phys. Rev. 161, 189 (1967).
[12]L. D. Landau and E. M. Lifshitz, *Statistical Physics* (Addison-Wesley, Reading, Mass., 1958), Sec. 10.
[13]V. K. Tkachenko, Zh. Eksp. Teor. Fiz. 49, 1875 (1965) [Sov. Phys.-JETP 22, 1282 (1966)].
[14]D. Stauffer and A. L. Fetter, Phys. Rev. 168, 156 (1968).
[15]S. J. Putterman, *Superfluid Hydrodynamics* (North-Holland, Amsterdam, 1974), Chap. VI.
[16]P. Mathieu, A. Serra, and Y. Simon, Phys. Rev. B 14, 3753 (1976).
[17]R. J. Miller, I. H. Lynall, and J. B. Mehl, Phys. Rev. B 17, 1035 (1978).
[18]See, e.g., F. K. Moore, *Theory of Laminar Flows* (Princeton University Press, Princeton, N.J., 1964), p. 99.